Simulated changes in atmospheric dust in response to a Heinrich stadial

Lisa N. Murphy,[1] Amy C. Clement,[1] Samuel Albani,[2] Natalie M. Mahowald,[2] Peter Swart,[3] and Monica M. Arienzo[3]

Received 14 August 2013; revised 26 November 2013; accepted 2 December 2013; published 15 January 2014.

[1] Heinrich stadials (HS), thought to be triggered by increased ice discharge in the high-latitude North Atlantic at glacial periods, resulted in large freshwater forcing that weakened the Atlantic Meridional Overturning Circulation (AMOC). These events are strongly expressed in paleoclimate records throughout the Atlantic basin and much of the tropics. Compared to the Last Glacial Maximum, recent proxy data suggest HS were much drier and dustier in large parts of the tropics. We use a global climate model coupled to a prognostic dust model to examine the response of dust to changes in climate during HS. Despite some significant changes in regional precipitation patterns in response to the simulated shift in the Intertropical Convergence Zone, we find that changes in winds have a larger effect on dust mobilization and deposition patterns than soil moisture or vegetation changes associated with a weaker AMOC. Although Europe was colder and drier during HS, the annual mean glaciogenic dust emission rate is lower because a southward shift in the Northern Hemisphere jet stream leads to weaker winds and less dust mobilization. The proximity of the westerly wind anomaly associated with the jet stream shift increases gustiness and dust mobilization over northwestern Africa and shifts the African Easterly Jet southward resulting in less African dust transport and deposition over the North Tropical Atlantic. Drier conditions over the Sahel region of North Africa, however, do not lead to increased dust mobilization in our model. When we perturb Sahelian soil characteristics, our results are in better agreement with proxies.

Citation: Murphy, L. N., A. C. Clement, S. Albani, N. M. Mahowald, P. Swart, and M. M. Arienzo (2014), Simulated changes in atmospheric dust in response to a Heinrich stadial, *Paleoceanography*, *29*, 30–43, doi:10.1002/2013PA002550.

1. Introduction

[2] Arid regions in North Africa and China have been major sources of dust for thousands [*de Menocal et al*., 2000] if not millions of years [*Guo et al*., 2004; *Schuster et al*., 2006]. While ice cores show the most dramatic increases in dust concentrations occur during times of glacial maxima, data throughout the tropics suggest it was drier and dustier during millennial-scale arid events, known as Heinrich stadials (HS) [*Tjallingii et al*., 2008; *Mulitza et al*., 2008; *Niedermeyer et al*., 2009; *Stager et al*., 2011; *McGee et al*., 2013]. Furthermore, records suggest dust deposition in the eastern tropical Atlantic during the most recent HS (HS1; 18–17 ka) was higher than at any time in last 50 kyr [*Jullien et al*., 2007; *Tjallingii et al*., 2008; *Mulitza et al*., 2008].

[3] HS are generally thought to be triggered by increased ice discharge in the high-latitude North Atlantic during glacial periods [*Heinrich*, 1988; *Bond et al*., 1992, 1993; *Manabe and Stouffer*, 1993; *Broecker*, 1998; *Grousset et al*., 2000; *Hemming*, 2004], which resulted in large freshwater forcing that weakened the Atlantic Meridional Overturning Circulation (AMOC) [*Vidal et al*., 1997; *Cortijo et al*., 1997; *McManus et al*., 2004]. HS1 led to an almost total collapse of the AMOC [*McManus et al*., 2004] and a bipolar temperature response [*Broecker*, 1998; *Stocker*, 1998; *Rahmstorf*, 2002; *Stocker and Johnsen*, 2003; *Lamy et al*., 2007; *Barker et al*., 2009]. In the Northern Hemisphere, proxies indicate Greenland's temperatures ranged from 2–8°C cooler during HS1 [*Cuffey and Clow*, 1997; *Masson-Delmotte et al*., 2005]. Although the North Greenland Ice Core Project temperature reconstruction shows little cooling during these HS periods [*Kindler et al*., 2013]. In the Southern Hemisphere, South Atlantic and Antarctic temperature proxies indicate a 1–3°C warming [*Lamy et al*., 2007; *Barker et al*., 2009]. Proxies throughout the Atlantic basin show changes that

[1]Rosenstiel School of Marine and Atmospheric Science, University of Miami, Miami, Florida, USA.
[2]Department of Earth and Atmospheric Sciences, Cornell University, Ithaca, New York, USA.
[3]Marine Geology and Geophysics Department, University of Miami, Miami, Florida, USA.

Corresponding author: L. N. Murphy, Rosenstiel School of Marine and Atmospheric Science, University of Miami, 4600 Rickenbacker Causeway, MPO, Miami, FL 33149-1098 USA. (lmurphy@rsmas.miami.edu)

0883-8305/14/10.1002/2013PA002550

are consistent with a southward shift in the Intertropical Convergence Zone (ITCZ) [*Peterson et al*., 2000; *Clement and Peterson*, 2008]. Numerous climate model simulations have tested whether freshwater discharge into the North Atlantic can explain the magnitude of the widespread climate changes indicated by paleoclimate records (see *Alley* [2007], *Clement and Peterson* [2008], *Chiang et al*. [2003], *Chiang and Bitz* [2005], and *Chiang* [2009] for reviews on this). It is well known that high-latitude cooling either by an AMOC collapse [*Vellinga and Wood*, 2002; *Zhang and Delworth*, 2005; *Broccoli et al*., 2006] or via the presence of sea ice or land ice sheets [*Chiang et al*., 2003; *Chiang and Bitz*, 2005] forces a southward shift of the ITCZ, which can strengthen the winter Northern Hemisphere (NH) Hadley cell circulation and shift the subtropical eddy-driven jet southward [*Lee and Kim*, 2003; *Kang et al*., 2009; *Frierson and Hwang*, 2012]. Models tend to show a robust shift in precipitation over the ocean; however, the precipitation signal over land is not as clear. Consequently, the widespread "pan-tropical drought" suggested by paleoclimate proxies is underestimated in climate models [*Stager et al*., 2011].

[4] Recent studies suggest African dust plays a role in driving 20th century sea surface temperature (SST) trends in the North Atlantic [*Foltz and McPhaden*, 2008a, 2008b; *Evan et al*., 2009, 2011, 2012], and that there is a positive feedback between North Atlantic SST, African dust, and Sahel rainfall on multidecadal timescales [*Evan et al*., 2011; *Wang et al*., 2012]. Observations indicate that at times when the North Atlantic is anomalously cold, the ITCZ shifts south, causing drying in the Sahel. This in turn increases dust emissions, which further cool the North Atlantic by scattering solar radiation [*Evan et al*., 2009, 2011; *Yoshioka et al*., 2007], thus leading to a positive feedback. Together, these prior studies suggest that in order to simulate North Atlantic SST changes, models must be able to correctly simulate the dust cycle and its interaction with the climate.

[5] While modern climate analyses suggest a possible feedback between dust and climate, most paleoclimate simulations have used prescribed dust or do not assess the two-way coupled dust-climate interactions [*Braconnot et al*., 2007]. Yet, the paleoclimate record shows significant millennial fluctuations in North African dust fluxes [*Mulitza et al*., 2008; *Tjallingii et al*., 2008; *Niedermeyer et al*., 2009; *Just et al*., 2012]. Here we use a state-of-the-art climate model to examine the two-way relationship between climate and dust during a HS and corroborate our results against proxy records. Our methodology is given in section 2; section 3 describes the climate response to HS as well as the dust-climate feedback, and our discussion and summary are detailed in section 4.

2. Experimental Design

[6] We perform experiments with the Community Climate System Model version 4 (CCSM4), a general circulation climate model consisting of atmosphere, ocean, land, and sea ice components that are linked through a coupler that exchanges state information and fluxes between the components (*Gent et al*., 2011). The atmospheric model is the Community Atmosphere Model version 4 (CAM4), which uses the Lin-Rood finite volume core with a $1.25° \times 0.9°$ uniform resolution and has 26 levels in the vertical. The land model is the Community Land Model version 4 (CLM4) [*Lawrence et al*., 2012], which uses the same horizontal resolution as CAM4. CLM4 includes improved hydrology and a carbon-nitrogen (CN) biogeochemistry model that affects seasonal and interannual vegetation phenology. The sea ice model is the Community Ice Code version 4 [*Hunke and Lipscomb*, 2008; *Holland et al*., 2012], which includes an improved radiative transfer scheme [*Briegleb and Light*, 2007] and explicitly allows for the incorporation of absorbers, such as black carbon and dust, in the radiation physics. We use the slab ocean model (SOM) version of CCSM4. In the SOM, the ocean heat transport convergence is prescribed as a Q-flux, which is constructed from fully coupled Last Glacial Maximum (LGM) simulation [*Brady et al*., 2013].

[7] Updates and improvements in the component model physics in CCSM4 have lead to improvements alleviating some regional biases for the preindustrial climate simulation discussed in *Neale et al*. [2013]. It is important to note that physical parameterizations or physical biases will impact our simulated climate response. An intermodel comparison using multiple GCMs and dust models, as well as a more thorough model-data comparison, can help reduce some of the uncertainty.

[8] Simulations are initialized using restart files from the fully coupled CCSM4 Last Glacial Maximum (LGM) CMIP5 simulation at the standard 1° resolution [*Brady et al*., 2013]. We follow the Paleoclimate Modeling Intercomparison Project (PMIP3) protocols for LGM forcings and boundary conditions [https://pmip3.lsce.ipsl.fr/wiki/doku.php/pmip3:design:lgm:final]. The land-sea mask is altered to include exposed land due to reduced sea level drop of approximately 120 m. Since PMIP3 does not specify a LGM vegetation distribution, the plant functional type distribution is fixed at preindustrial conditions [*Lawrence and Chase*, 2007]. However, the CN biogeochemistry model allows for prognostic vegetation phenology. Total leaf and stem area indices (LAI and SAI) and canopy heights are prognostic and are dependent on the simulated LGM climate state. In our LGM simulation, the Bering Strait is closed and the Indonesian Archipelago Maritime Continent replaces the shallow waters currently present.

[9] To test how these climate changes impact the dust loading, transport, and deposition, we couple CCSM4 to a prognostic dust based on the dust source, transport, and deposition model used in *Mahowald et al*., 2006 and S. Albani (in revision, 2013). Dust impacts climate through the scattering and absorption of both shortwave and longwave radiation, surface and cloud albedo effects and by adding nutrients (Fe, P) to the biosphere. New updates to dust optics and size distributions [*Kok*, 2011; S. Albani in revision, 2013] make dust more reflective in the shortwave. The model has a fixed size distribution at emission, but the dust is allowed to evolve in size as it is transported away from the source regions. The fixed size distribution at the source assumes the mechanism for dust entrainment is saltation, and therefore it focuses on the "fine" dust. The fixed size distribution is based on *Kok* [2011], and limited to 0.1–10 μm, since atmospheric concentration observations are restricted to this size, and most of the long-range transport is in this size. However, there are solid observations showing larger particles making it fairly far from the source regions [e.g., *Reid et al*., 2003; *Lawrence and Neff*, 2009]. Dust is mobilized when the wind reaches a threshold velocity, is then uplifted

Table 1. Description of the Experiments Conducted in This Manuscript

Simulation Name	Hosing	Dust-Radiative Effect	Perturbed Soil Erodibility
LGM	No	Yes	No
LGM Hose	Yes	Yes	No
LGM Hose NoDRE	Yes	No	No
LGM Hose Perturb	Yes	Yes	Yes

by dry convection and transported by the mean circulation. Dust falls out through both wet deposition, which includes in-cloud and below-cloud scavenging, and dry deposition, including gravitational fall out and turbulent mix-out processes [*Zender et al*., 2003a]. Observations over the open ocean suggest dominance of wet deposition over dry deposition at most stations [e.g., *Mahowald et al*., 2011, QSR Table 3], although this model is a bit too high [*Mahowald et al*., 2011].

[10] LGM simulations include glaciogenic dust sources [*Mahowald et al*., 2006] and were calibrated to match available dust records from the Dust Indicators and Records of Terrestrial and Marine Palaeoenvironments version 3 (DIRTMAP3) [*Maher and Kohfeld*, 2009], as described in S. Albani (in revision, 2013). DIRTMAP3 includes dust deposition data from ice cores, marine sediment traps, and marine sediment cores for both the modern and LGM. To compare simulated versus observed dust fluxes for the LGM and present, *Mahowald et al*. [2006] and S. Albani (in revision, 2013) modify the mass accumulation rate (MAR) calculation by including only those particles that are less than 10 μm in diameter, which is the particle size range that would have significant radiative transfer effects in the atmosphere [*Tegen*, 2003], as well as the particle sizes used in the model.

[11] Dust emissions in this model are assumed to scale with the cube of wind speed, as stronger winds have more energy available for particle entrainment and create additional fine particles by breaking up soil aggregates [*Zender et al*., 2003a]. The most important factors for the mobilization, or entrainment of dust into the atmosphere, are the wind friction speed, vegetation cover, snow cover, surface soil moisture, and soil erodibility [*Zender et al*., 2003a]. All but the last variable are time and spatially varying variables used or derived in the land model. Differences in soils' susceptibility to erosion (i.e., related to soil grains size and textures) are summarized in a multiplicative parameter for the dust flux, the geomorphic soil erodibility [*Zender et al*., 2003b], and are based on the concept of preferential sources [*Ginoux et al*., 2001]. This is a spatially-varying scale factor for dust emissions, which is based on the regional topography and accounts for the concept that topographic lows are hot spots for dust production [*Prospero et al*., 2002; *Zender et al*., 2003b]. This parameter, which is applied in the atmospheric component of our model (CAM), indicates the relative effectiveness of each grid box for causing dust generation. A major source of uncertainty in dust models is represented by the magnitude and location of the emissions [e.g., *Cakmur et al*., 2006; *Shao et al*., 2011; *Huneeus et al*., 2011]. S. Albani (in revision, 2013) reviewed available information of dust provenance, for both present/interglacial and LGM climates, in order to help refine the soil erodibility maps to represent the relative intensity of different source areas. In tuning the LGM soil erodibility, S. Albani (in revision, 2013) tried to match the flux of the fine dust as best as possible. Different interpretations of the observed terrigenous sediments from marine cores do exist, though. Mobilization increases with increasing wind friction velocity cubed and decreasing vegetative cover and soil moisture. In CLM, the transpiration beta factor (BTRAN) parameter represents soil moisture limitation on vegetative growth. BTRAN ranges from one when soil is wet to near zero when soil is dry and depends on root distribution of the overlying vegetation and soil water potential for each soil layer.

[12] We run four CCSM4-SOM simulations with the prognostic dust model to examine the impact of HS on the dust cycle and climate: LGM, LGM Hose, LGM Hose no dust radiative effect (NODRE), and LGM Hose Perturb (Table 1). In these CCSM4-SOM simulations, Q-flux is constructed from a 20 year climatology of SST, mixed-layer depth, and air-sea fluxes from the equilibrated fully coupled LGM simulation (model years 980–999). Q-flux is constructed to reproduce the SST and sea ice of the fully coupled simulation using a new formulation of the mixed-layer in CCSM4 documented in *Bitz et al*. [2012]. Our LGM simulation is our control simulation that takes into account all LGM boundary conditions and forcings, as in the fully coupled simulation. In our idealized freshwater hosing experiment, LGM Hose, we add a $25\,W\,m^{-2}$ cooling flux to the prescribed Q-flux in the North Atlantic (50–70°N, 70°W–15°E), and a compensating $0.65\,W\,m^{-2}$ warming flux to all Southern Hemisphere ocean grid cells. We chose these flux values because they resulted in the climate response that best matched observations [*Rühlemann et al*., 1999; *Bard et al*., 2000; *Kim et al*., 2002; *McManus et al*., 2004; *Clement and Peterson*, 2008]. Doubling our prescribed flux anomalies led to too strong warming in the SH and a large sea ice feedback, whereas roughly half that amount did not cool the North Atlantic sufficiently compared with observed HS [*Clement and Peterson*, 2008]. We examined the Q-flux among different coupled models and different versions of the same model and found the changes in Q-flux in response to freshwater input were not statistically significant since the spread between different models and versions of the same model were considerably large. Therefore, we determined the simplest way to redistribute heat and maintain energy balance was to redistribute a small amount throughout the entire Southern Hemisphere. The prescribed Q-flux is highly idealized since we are not accounting for regional patterns in the global oceanic circulation, but the overall effect in previous work [*Zhang and Delworth*, 2005; *Stouffer et al*., 2006] shows that the warming spreads in most locations in the Southern Hemisphere. Although we produce a static response in the Southern Hemisphere to an AMOC collapse, the effect of advection and wave mechanisms redistributing heat in the ocean [*Johnson and Marshall*, 2002; *Dong and Sutton*, 2002; *Speich et al*., 2007] does not disagree with our approach.

[13] We run an additional simulation in which dust is made radiatively inactive, or no dust radiative effect (NODRE), LGM Hose NODRE. In this simulation we remove dust from the radiative heating rate calculation. This allows us to quantify the effect of the radiative forcing of dust during HS. Finally, we run an additional simulation in which we increase the soil erodibility over the Sahel region of North Africa (between 13 and 20°N), LGM Hose Perturb, to account for a possible southward shift in the Sahara-Sahel

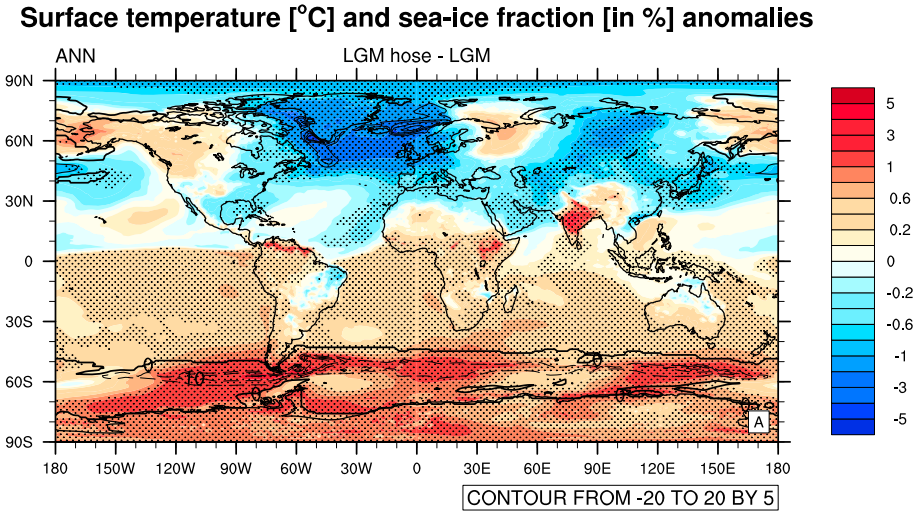

Figure 1. Simulated annual mean (ANN) surface temperature (°C; colored contours) and sea ice fraction (in %; contour lines) anomalies between the LGM_Hose and LGM (LGM_Hose-LGM) experiments. The contour interval for sea ice is 5%. Statistically significant differences in surface temperature based on a Student's *t* test are stippled and overlaid on the contours.

Border during the last HS [*Michel*, 1973; *Collins et al*., 2013]. This is a branch simulation that is initialized with conditions from our equilibrated LGM Hose simulation, and it is run for an additional 15 years. The first five are disregarded as spin up. The other simulations (LGM, LGM Hose, and LGM Hose NODRE) were integrated for 45 years and climatological seasonal and annual means were calculated over the last 20 years. A Student's *t* test is used to determine if the differences between our simulations are indistinguishable from unforced internal variability in the model. The internal variability is derived from our control LGM simulation. Statistically significant differences with $p \leq 0.05$ are stippled in the figures. An outline of the experiments is given in Table 1.

3. Results

3.1. Atmospheric Circulation Response

[14] First we consider the idealized effect of North Atlantic meltwater ice on glacial climates in our model simulations (LGM Hose—LGM). Consistent with proxy records [*Lamy et al*., 2007; *Barker et al*., 2009], the idealized hosing experiment results in an interhemispheric temperature asymmetry [*Broecker*, 1998] with strong cooling in the North Atlantic and warming throughout the Southern Hemisphere (Figure 1). Although proxy records indicate regions of warming in the SH [*Lamy et al*., 2004], the broad warming seen in our simulations is due to the prescribed Q-flux changes and not necessarily in agreement with proxy data. Although, our results are comparable to a more realistic hosing experiment using the older version of the fully coupled model (CCSM3) [*Otto-Bliesner and Brady*, 2010]. HS reduce the northward heat transport in the ocean and leads to a 2–4°C cooling in high-latitude NA glacial SSTs. The SH is warmest during boreal summer and the warmest SSTs are in the Southern Ocean, where there is sea ice loss. The strongest cooling coincides with regions of sea ice expansion, located near the southern edge of the Labrador Sea and within the Norwegian Sea. This is consistent with other modeling results that show the strongest cooling associated with Heinrich events is southeast of Greenland [*Ganopolski and Rahmstorf*, 2001]. Cooler temperatures extend eastward throughout the northern high to middle latitudes, consistent with previous studies [*Ganopolski et al*., 1998; *Chiang and Bitz*, 2005; *Zhang and Delworth*, 2005; *Lee et al*., 2011]. A horseshoe shaped region of cooling extends along the Iberian coast and African coastline and extends westward across the tropical Atlantic, consistent with observations

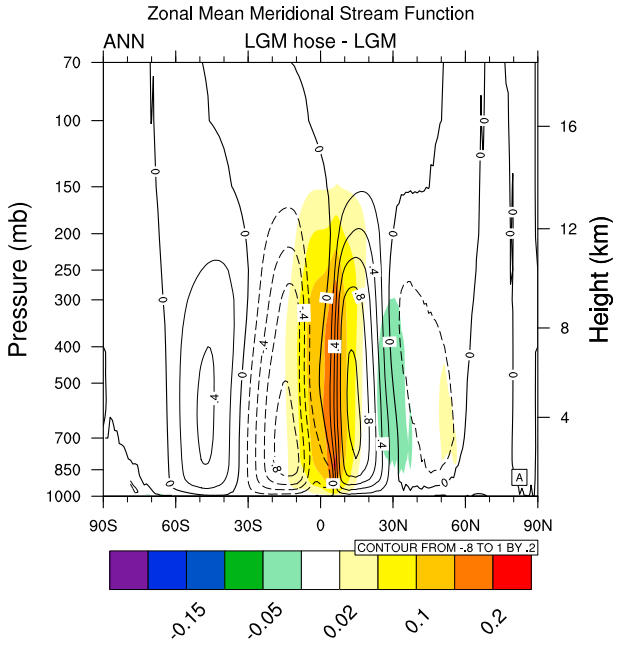

Figure 2. Simulated annual mean (ANN) meridional circulation (contour unit $\times 10^{11}$) anomalies between the LGM_Hose and LGM experiments (colored contours). The annual mean meridional circulation for the LGM experiment is overlaid on the colored contours (interval from -0.8 to 1 by 0.2 kg s^{-1}).

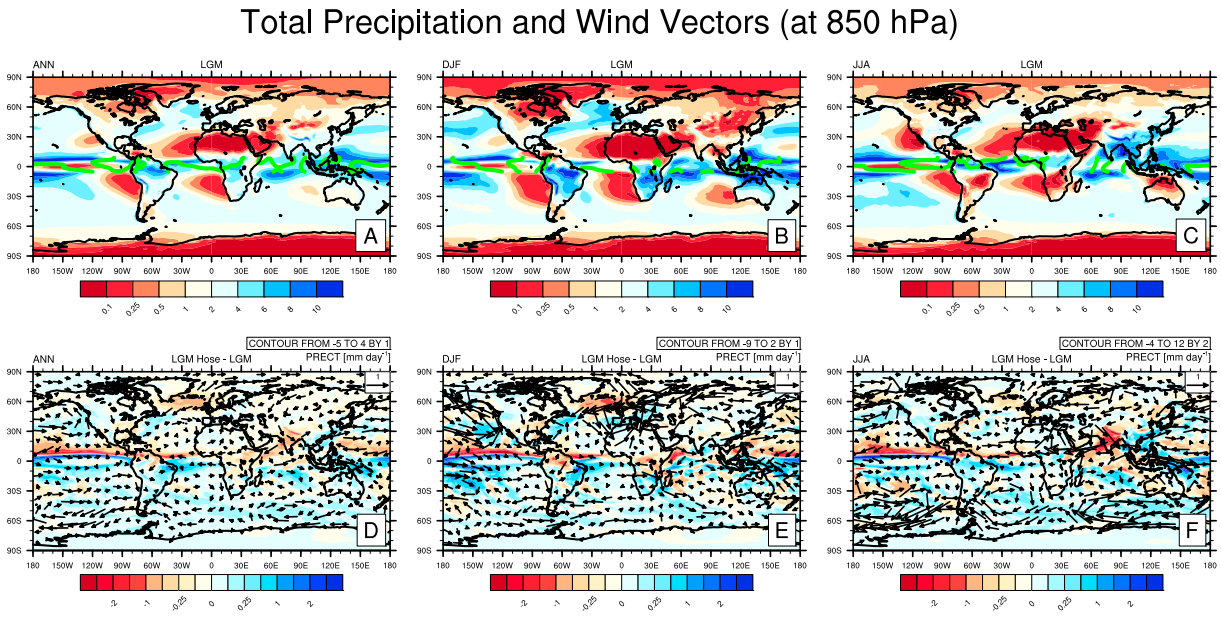

Figure 3. (a) Annual mean (ANN), (c) boreal winter (December-January-February), and (c) boreal summer (June-July-August) simulated precipitation (mm d^{-1}) at the LGM and (d, e, and f, respectively) the anomalies between the LGM_Hose and LGM experiments. The green line shows the zero crossing point of meridional wind data as indicators for ITCZ location. Anomalous wind vectors at 850 hPa (in black) are overlaid on seasonal precipitation anomalies (Figures 3d–3f).

[*Zhao et al*., 1995]. Although there are some warmer regions in the NH, they are not statistically significant.

[15] HS result in a southward shift in the Northern Hemisphere Hadley and Ferrel cells (Figure 2), consistent with the simulated shift in the Intertropical Convergence Zone (ITCZ) toward the warmer Southern Hemisphere (Figure 3d), and in agreement with other studies of extratropical NH cooling [*Kang et al*., 2009; *Lee et al*., 2011; *Frierson and Hwang*, 2012]. Additionally, the NH midlatitude jet stream shifts equatorward during HS (Figure 4), consistent with studies that show a southward expansion of the polar zone during the glacial period [*Chapman and Maslin*, 1999; *Kageyama et al*., 1999; *Otto-Bliesner et al*., 2006; *Braconnot et al*., 2007] and other studies that show a northward shift in the jets under global warming [*Yin*, 2005; *Lorenz and DeWeaver*, 2007; *Chen et al*., 2008; *Lu et al*., 2008; *Kang and Lu*, 2012]. The upper troposphere jet is also associated with the storm track and midlatitude precipitation maximum, thus a southward shift in the jets brings less precipitation to NH high-latitude North Atlantic and parts of western Europe and more precipitation to the Iberian coast, the Mediterranean, and NW Africa, especially in winter (Figure 3e). Drying occurs in the high-latitude North Atlantic where we prescribed cooling and between the Equator and 30°N with the exception of Southeast Asia. The Gulf Stream is wetter in the annual mean and is related to a stronger subtropical high in the North Atlantic during the summer, which leads to greater evaporation and precipitation in the Gulf Stream region. Statistically significant drying occurs over Central Africa and the Eastern U.S. In Africa, most of the drying is related to reduced precipitation in the winter (Figure 3e). In the summer, a reversal in the Asian monsoonal flow brings more moisture to North and Central Africa and therefore higher precipitation (Figure 3f).

[16] In South America, changes in precipitation are consistent with proxy records and the southward shift in the ITCZ. The Cariaco Basin and Amazon region is drier, while Northeastern Brazil becomes much wetter (Figure 3d)

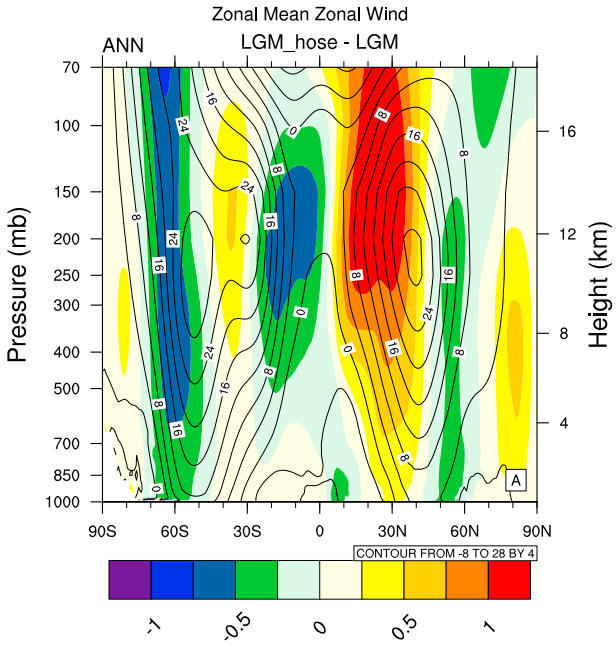

Figure 4. Annual (ANN) zonal mean zonal wind anomaly between the LGM_Hose and LGM experiments (colored contours). The annual zonal mean zonal wind for the LGM experiment is overlaid on the colored contours (interval from −8 to 28 by 4 m s^{-1}).

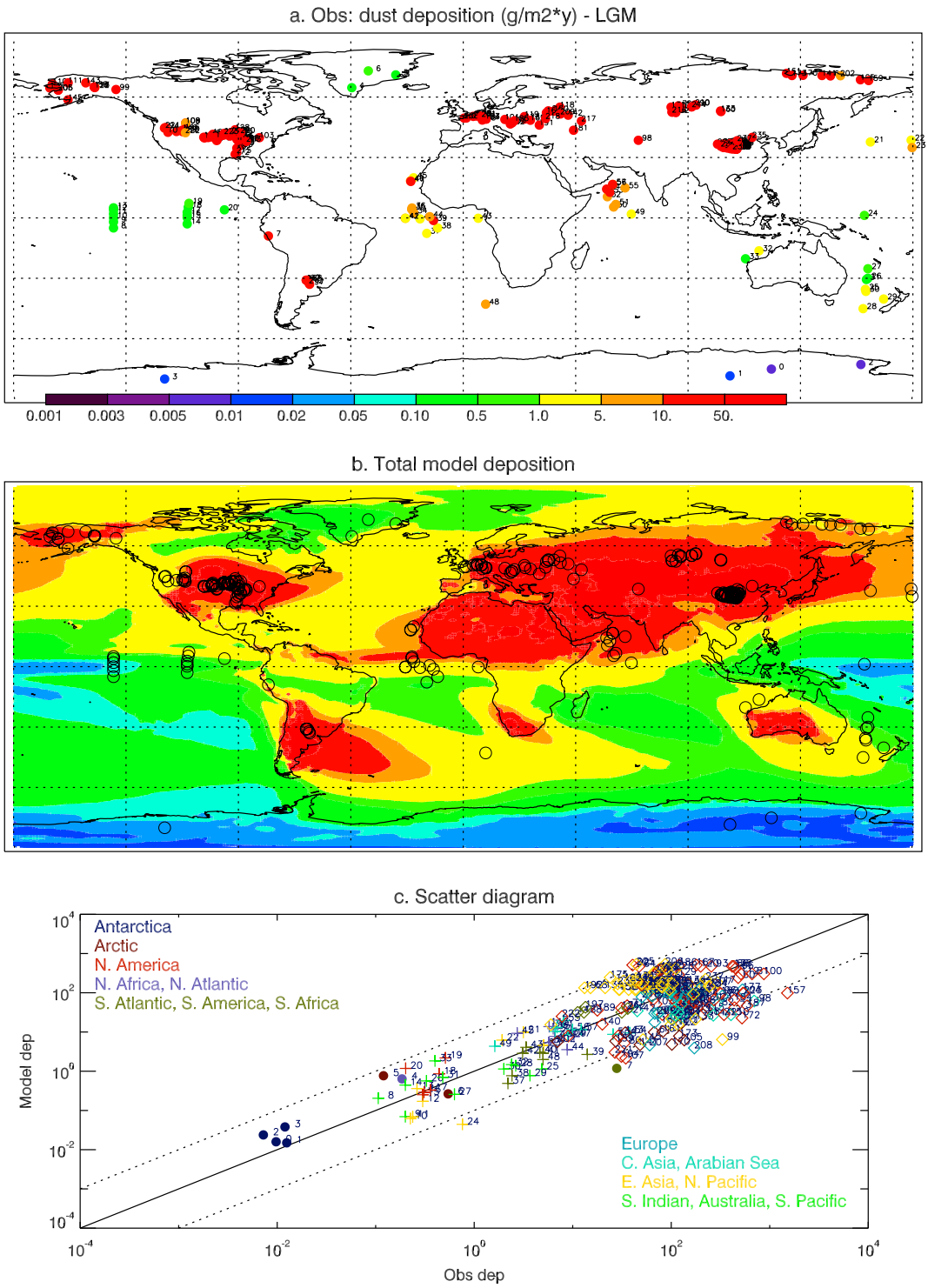

Figure 5. (a) Observed and (b) modeled dust deposition ($g\,m^{-2}\,yr^{-1}$) for the LGM simulation, and (c) a model versus observations scatterplot. Locations of observational sites are clustered in the scatterplots based on their geographical location.

[*Peterson et al.*, 2000; *Wang et al.*, 2004; *Clement and Peterson*, 2008; *Hessler et al.*, 2010]. Our model also produces much wetter conditions over Indonesia that is in agreement with proxy data showing increased plant cover and decreased grass cover signifying wetter conditions during HS1 [*Van der Kaars et al.*, 2001; *Turney et al.*, 2006]. With the exception of eastern China, which shows wetter conditions in the annual mean although the changes are not statistically significant, the overall spatial pattern of drying is consistent with paleohydrological data shown in *Stager et al.* [2011].

[17] In the SH, the midlatitude jet stream is constricted, and there is a weakening of the Southern Ocean westerlies (Figure 4). A reduction in the annual mean zonal wind in the SH is due to a reduction in the meridional temperature

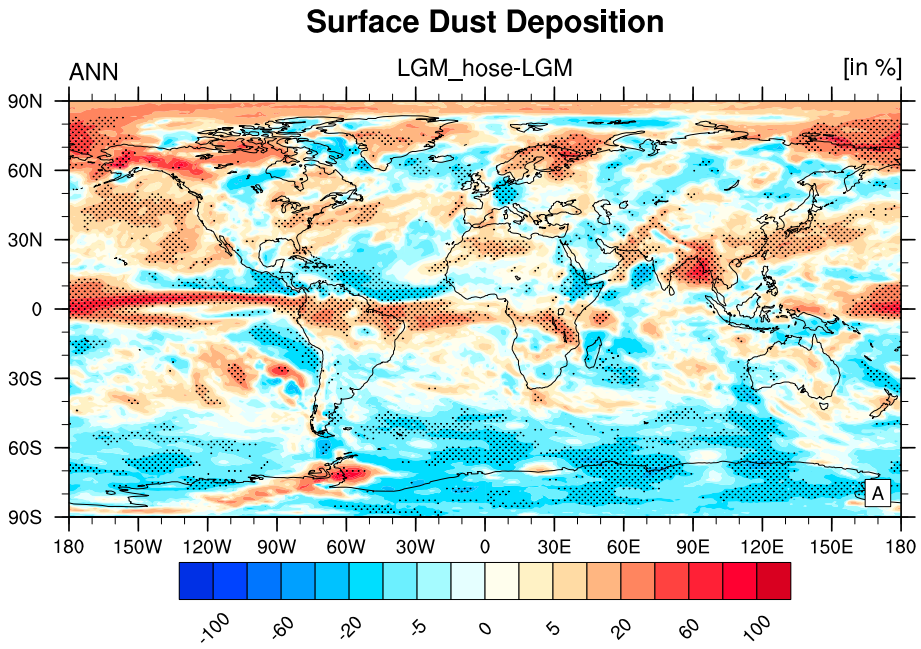

Figure 6. Simulated annual mean (ANN) dust deposition (in %) anomalies between the LGM_Hose and LGM (LGM_Hose-LGM) experiments. Statistically significant differences in dust deposition based on a Student's *t* test are stippled and overlaid on the contours.

gradient due to increased oceanic heat flux into the SH. This disagrees with *Lee et al*. [2011], which shows a strengthening of Southern Ocean westerlies in a HS-like experiment. This disparity may arise because *Lee et al*. [2011] did not change the oceanic heat flux outside of the North Atlantic. We believe our results are more realistic since less northward oceanic heat transport would be compensated by increased heat transport to the SH, as simulated in coupled models [e.g., *Zhang and Delworth*, 2005].

3.2. Dust Response

[18] In making comparisons between model outputs and dust observations and/or archives (e.g., sediment cores), it is important that size fractions are matched. This is achieved by estimating the MAR for particles < 10 μm for a number of loess sites around the world. Comparisons of our simulated LGM dust deposition to estimates from the DIRTMAP3 database show that the model does a good job simulating the observed dust deposition during the LGM (Figure 5).

[19] The simulated annual mean dust deposition responds to climate change during HS by decreasing dust deposition in the tropical North Atlantic (TNA) and increasing dust deposition in the tropical South Atlantic, Northeastern Brazil, and in the Amazon forest (Figure 6). In the eastern equatorial Pacific Ocean there is a large increase in dust deposition along the equator and reduced dust deposition to the north and south. Further analysis shows that these results are due to changes in wet deposition owing to the shift in the ITCZ (Figures 3d and 6).

[20] More dust deposition occurs over northwestern Africa, which is related to stronger winds due to the southward shift in the westerly winds, especially in winter (Figure 3e). Dust emissions scale with wind speed and stronger winds results in greater dust emission and deposition over this region. Higher dust deposition off the NW African coast during winter is in agreement with sediment trap data [*Bory and Newton*, 2000].

[21] Dust loading and deposition over much of the subtropical North Atlantic is lower in our Heinrich simulation compared to our LGM simulation (Figure 6 shows the decrease in dust deposition and Figure 7b shows the decrease in aerosol optical depth). A southward shift in the African Easterly Jet (AEJ) (seen in Figure 7b, wind anomalies at 700 hPa) reduces dust transport across the subtropical North Atlantic and Caribbean. This is evident in the aerosol optical depth anomaly, which shows reduced optical depth over the TNA between 0–30°N and greater optical depth in the equatorial Atlantic from 5°N to 5°S where the easterly winds are increased (Figure 7b).

[22] Next, we examine how dust mobilization changed by looking at area averaged anomalies of wind, vegetation cover represented as Total Leaf Area Index (TLAI), BTRAN, and dust emission rate in five different regions: North Africa, North America, Europe, South America, and Australia (Figure 8).

[23] Since the area-averaged BTRAN and LAI are reduced throughout the year over North Africa we would expect an increase dust emission from this region. Although emissions from northwestern Africa (near Morocco) are higher throughout the year, the annual mean dust emission averaged over all of NA (north of 13°N) is increased by less than 2% in our HS simulation compared to our LGM simulation (Figure 8). A small increase in dust emissions is due to an increase in wind speed during the spring. North African dust emissions in our HS simulation are reduced throughout the remainder of the year. This suggests in the Saharan Desert, surface wind changes are more important than vegetative and soil moisture impacts in mobilizing dust.

[24] Drier conditions in the Sahel result in less evaporational cooling and warmer surface temperatures, and consequently

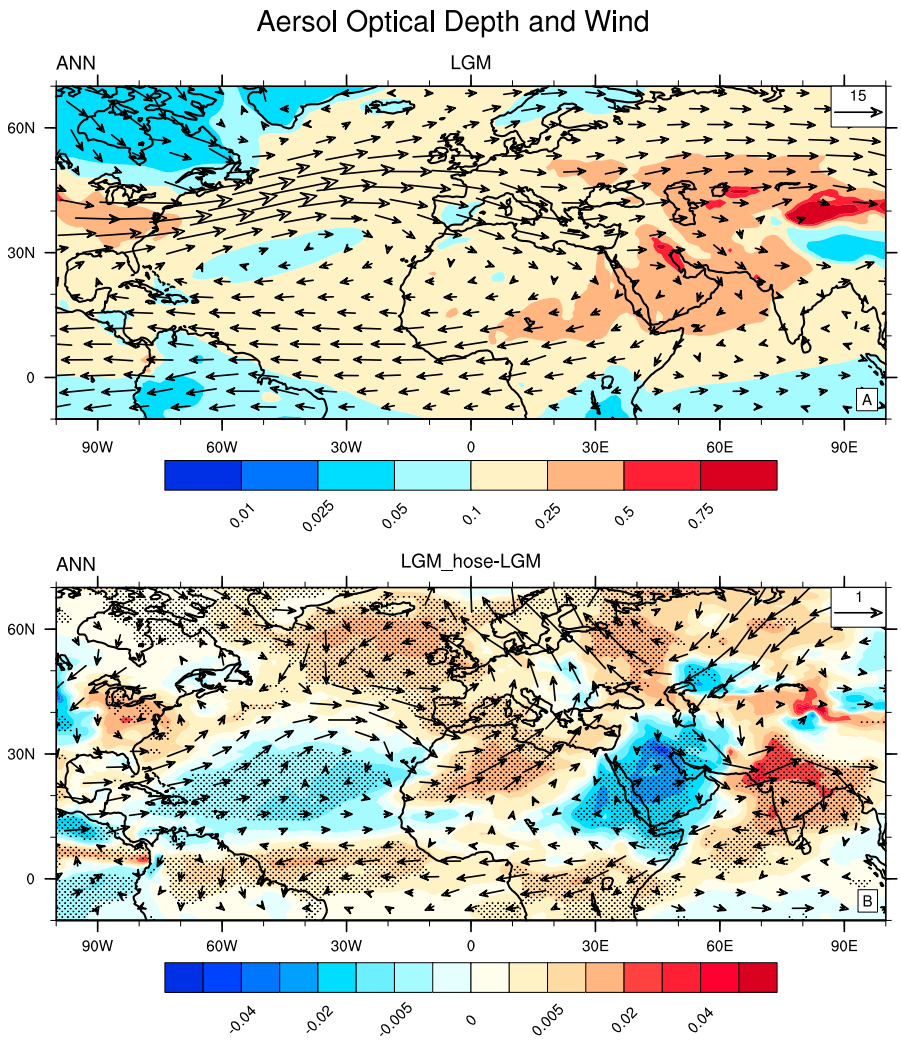

Figure 7. (a) Simulated annual mean (ANN) aerosol optical depth (in %; contour lines) for the LGM experiment and (b) the difference between the LGM_Hose and LGM (LGM_Hose-LGM) experiments. Statistically significant differences in aerosol optical depth based on a Student's *t* test are stippled and overlaid on the contours in Figure 7b. Mean (Figure 7a) and anomalous (Figure 7b) wind vectors at 700 hPa are overlaid on the figures.

decreases the meridional temperature gradient in North Africa (Figure 1). Although the Sahel region is drier, only regions with easily erodible soils can be strong sources [*Zender et al*., 2003b], and in our model during the LGM much of the Sahel is not assumed to be easily erodible.

[25] Most of the SH is wetter, with the exception of Southern Africa, which remains dry (Figure 3). Unlike *Mulitza et al*. [2008], our results show drying throughout most of Central and Southern Africa in the annual mean (between 20°S and 20°N) (Figure 3d). However, the summer appears to be wetter (Figure 3f). In addition, we see significant drying over India and the Arabian Sea, which is related to the shift in the Hadley cell, and is consistent with proxy data implying a severe reduction in the summer monsoon and wind activity in the Arabian Sea [*Kutzbach and Guetter*, 1986; *Schulz et al*., 1998; *Rashid et al*., 2007, 2011; *Sirocko et al*., 2000]. A band of higher dust deposition over the western Arabian Sea is in agreement with proxy data from *Sirocko et al*. [2000].

[26] In our LGM and LGM Hose simulations, dust emissions from North America and Europe are lowest in winter and highest in the summer (not shown). Over Europe, the southward shift in the storm track brings drier conditions and weaker winds throughout most of the year. The annual mean dust emission from LGM glaciogenic European dust sources over the entire domain is reduced by 6% (Figure 8). Results show reduced dust emissions during spring (March–May) although there is a 10% increase in wind speed during this season. We report a box area average and there is some spatial heterogeneity in the emissions. While dust emissions over Western Europe are decreased throughout the year, Eastern European dust emissions are higher in spring and fall (September–November).

[27] Drier and windier conditions in central and eastern North America results in a small (4%) increase in dust emission rates (Figure 8). Higher North American dust mobilization leads to more dust deposition off the eastern coast extending from the Bahamas and following the Gulf Stream

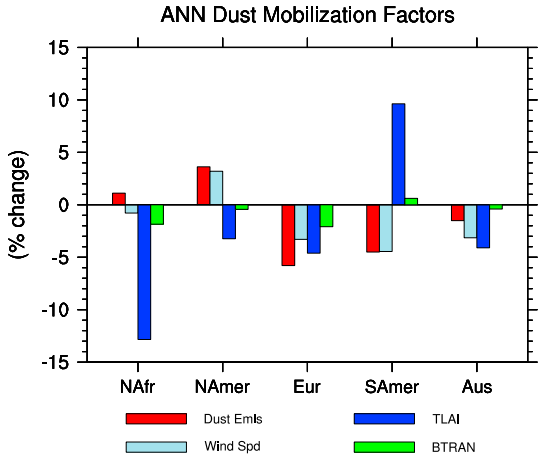

Figure 8. Bar chart of the percent change in annual mean (ANN) dust emission rates (g m^{-2} yr^{-1}) and dust mobilization factors (wind speed (m s^{-1}), TLAI, and BTRAN) between the LGM_Hose and LGM (LGM_Hose-LGM) experiments.

across the North Atlantic to the Bay of Biscay. The largest increase in dust deposition off the Eastern coast occurs in fall when the wind speed is increased. In addition to higher dust concentrations over the Gulf Stream, the annual mean high and low cloud amounts also increase.

[28] The annual mean dust emission rate in Australia is reduced by just 2% (Figure 8). Although drier conditions are found over Australia, weaker winds mobilize less dust. Wetter conditions and weaker winds work together to decrease dust emission from South America. Furthermore, less dust is deposited in the Southern Ocean and over Antarctica in the model. Lower dust fluxes over Antarctica is consistent with dust MAR in the European Project for Ice Coring in Antarctica Dome C ice core that shows higher fluxes during the LGM and lower dust fluxes since then [*Martínez-Garcia et al.*, 2011].

3.2.1. Dust-Climate Feedback

[29] Here we analyze the dust impact on climate by comparing our hosing run (LGM Hose) with dust radiatively active to a similar run in which dust does not influence

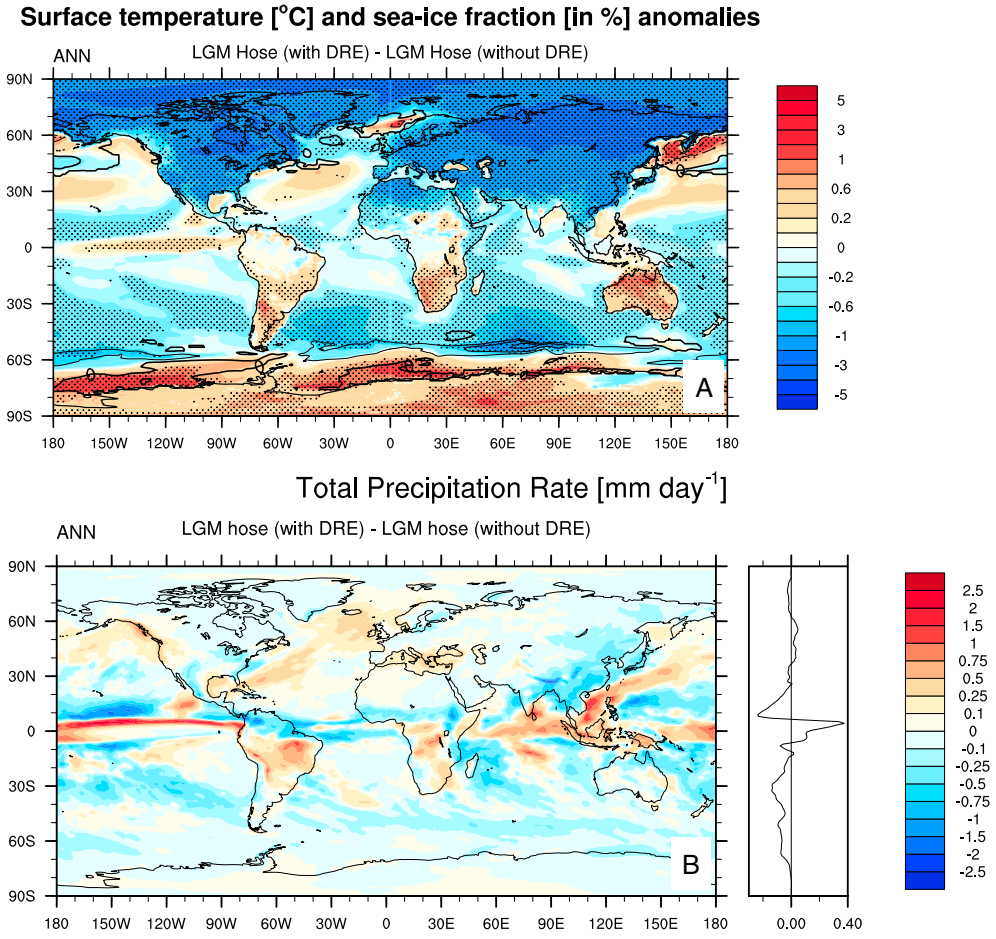

Figure 9. (a) Simulated annual mean (ANN) surface temperature (°C; colored contours) and sea ice fraction (in %; contour lines) anomalies and (b) precipitation (mm d^{-1}) anomalies between the LGM_Hose (with DRE) and LGM_Hose (without DRE) experiments. The contour interval for sea ice in Figure 9a is 5%. On the right side of Figure 9b we plot the zonal mean change in precipitation at each latitude.

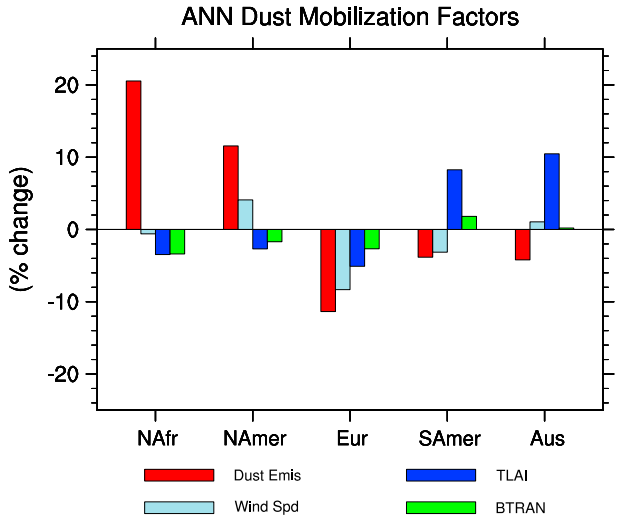

Figure 10. Bar chart of the percent change in annual mean (ANN) dust emission rates ($g\,m^{-2}\,yr^{-1}$) and dust mobilization factors (wind speed ($m\,s^{-1}$), TLAI, and BTRAN) between the LGM_Hose_Perturb and LGM_Hose (LGM_Hose_Perturb-LGM_Hose) experiments.

the radiation equation (LGM Hose NODRE). Results show that the climate response to the radiative forcing of dust during HS causes an additional cooling over the tropical and subtropical NA (Figure 9a). The tropical-subtropical North Atlantic is cooled by roughly 0.2°C. The SST cooling in response to DRE is slightly smaller than other studies [*Evan et al.*, 2009; *Mahowald et al.*, 2010; *Martinez Avellaneda et al.*, 2010; *Evan et al.*, 2012], or studies with our previous model version [e.g., *Yoshioka et al.*, 2007]. Modeled direct radiative forcing of dust is strongly sensitive to the optical properties and size distribution used. Additionally, the details of the modeled size distribution and dust optical parameters are very sensitive to the interplay of different processes that are still very uncertain. The DRE reduces the annual mean NH temperature by 0.97 K.

[30] These results suggest dust may amplify the climate response to a HS by enhancing NH and NA cooling, which can further shift the ITCZ southward and dry North Africa. This precipitation shift is seen over Africa (Figure 9b). Modeling studies indicate dust is responsible for up to 30% of the observed precipitation reduction in the Sahel, while SSTs are responsible for roughly 50% of the Sahel

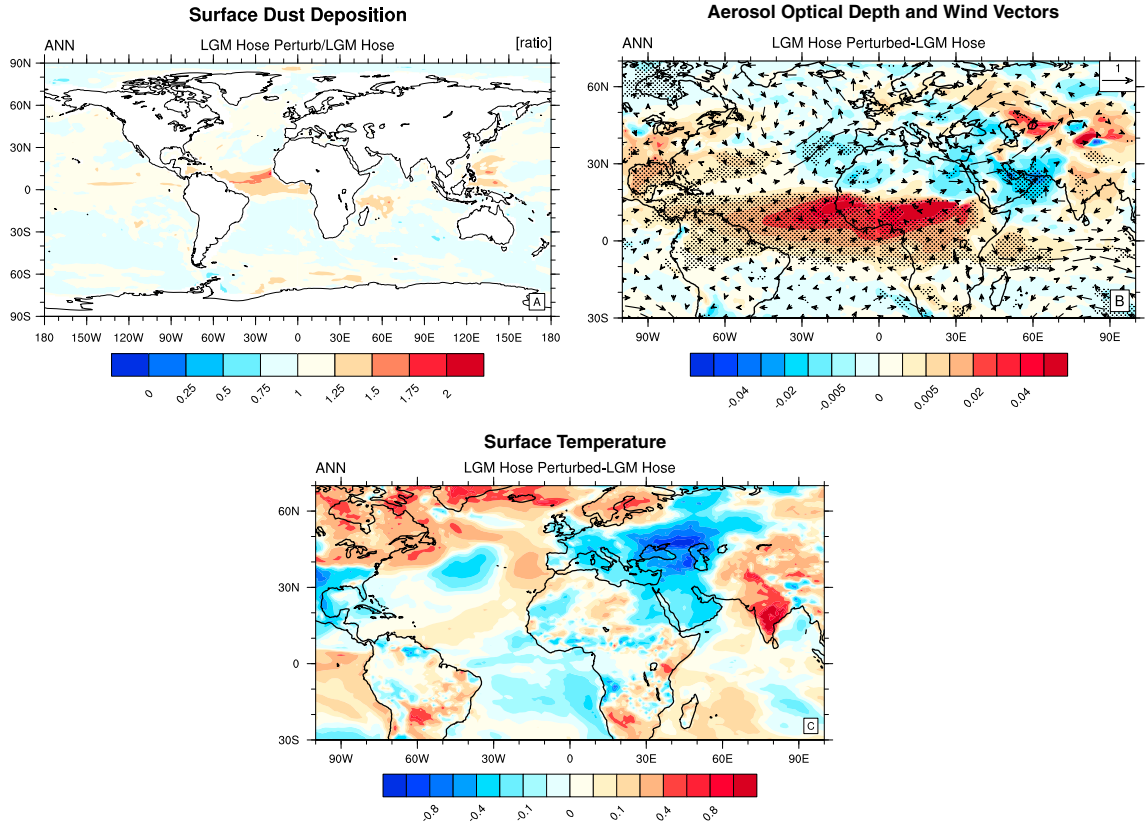

Figure 11. Simulated annual mean (ANN) surface temperature (°C; colored contours) and sea ice fraction (in %; contour lines) anomalies between the LGM_Hose and LGM (LGM_Hose-LGM) experiments. The contour interval for sea ice is 5%. Statistically significant differences in surface temperature based on a Student's *t* test are stippled and overlaid on the contours.

precipitation signal [*Yoshioka et al*., 2007]. However, shifts in the ITCZ due to dust is highly sensitive to how dust in parameterized in climate models [*Miller et al*., 2004]. In our study, the DRE contributes just a 4% reduction in Sahel precipitation during HS.

3.2.2. Perturbed Soil Erodibility

[31] In contrast to recent paleo-observational studies that show between a 2.5 [*McGee et al*., 2013] and eightyfold increase [*Just et al*., 2012] in dust flux into the eastern tropical-subtropical North Atlantic during HS1, our HS simulations show a negative annual mean dust flux anomaly over much of the tropical North Atlantic, with the exception of a small area of ~5–10% increase in dust flux off the coast of Mauritania (Figure 6). The magnitude of increased dust deposition is much smaller than what proxies suggest. Although geological sediments suggest there was an increase in coarse-sized dust particles during HS1, we would also expect the flux of fine particles to increase as well, since dust emissions scale with wind speed. In comparing modeled versus observed dust flux variability, we assume that total change in dust flux is also quantitatively representative for the fine ($<10\,\mu m$) dust fraction. While there is uncertainty in this assumption, we believe the uncertainty is likely no larger than the uncertainty already existing in reproducing (or estimating from some of the observations) the glacial-interglacial ratio of dust deposition. Since the hydrological conditions over North Africa result in less rainfall, drier soils, and reduced vegetation (shown as TLAI), which would increase dust emission, this suggests that the modeled dust emission is most sensitive to wind velocity and the prescribed soil erodibility.

[32] Relic Ogolian Dunes [*Michel*, 1973] occupied much of Senegal between 19 and 15 ka. The existence of these dunes as far south as 13°N suggests a southward shift in the Sahara-Sahel border occurred during this time [*Mulitza et al*., 2008; *Collins et al*., 2013]. Since the soil erodibility is assumed to be small in our model during the LGM, we run an additional simulation in which we perturb the soil erodibility over the Sahel region between 13 and 20°N. Over regions where the soil erodibility factor was zero, we increase it to a value of 0.1, this represents a 10% increase in the area average North African soil erodibility factor.

[33] The new Sahel dust source leads to a 20% increase in the annual mean dust emission rate (Figure 10), and a factor of 1.25–1.75 increase in dust deposition in the eastern tropical Atlantic between 5°S and 15°N (Figure 11). We also see a large increase in dust deposition in the western Caribbean Sea but little change in the Bahamas where speleothems suggest greater dust deposition during HS (Figure 11a) [*Arienzo et al*., 2011]. Aerosol optical depth is increased between 10°S and 20°N from Africa westward into South America. Aerosol optical depth is also increased over the Eastern U.S., Gulf of Mexico, and western North Atlantic. This is most likely due to higher dust emission from North America (Figure 11).

[34] The climate response to an increase in dust from the Sahel includes cooling of equatorial Atlantic where dust deposition is higher (Figure 11c). Cooler surface temperatures spread toward the southeastern subtropical South Atlantic and are related to increased cloud amount and reduced radiation at the surface (not shown). A coherent precipitation response was not found.

4. Summary and Discussion

[35] Our results show that HS can alter dust loading, transport, and deposition through changes in the mean climate state. A southward shift in NH storm tracks and changes in gustiness, in particular, have large impacts on dust mobilization over NH source regions. The similarities in the atmospheric response to HS between our idealized simulations and those using an ocean general circulation model with ocean dynamics [*Dong and Sutton*, 2002; *Zhang and Delworth*, 2005; *Stouffer et al*., 2006] give confidence in our method.

[36] The statistically significant (based on a Student's *t* test) changes in dust loading and dust deposition due to HS are the following:

[37] 1. There is a small increase (1.5%) in the annual mean dust emission rates from North Africa, which is due to surface wind changes and not vegetation or soil moisture changes. Dust emissions over North Africa are increased during the spring but reduced throughout the rest of the year. Since the summertime AEJ is a pathway of dust export out of Africa and across the Atlantic [*Jones et al*., 2003], anomalous westerly winds and a southward shift in the AEJ reduce dust deposition across the Atlantic and into the Caribbean. This is evident in the aerosol optical depth anomaly, which shows reduced optical depth over the TNA between 0 and 30°N and greater optical depth in the equatorial Atlantic from 5°N to 5°S where the easterly winds are increased (Figure 7b). A strengthening and southward shift in the AEJ during HS was previously seen in the modeling study of *Mulitza et al*. [2008]. A narrow region off the coast of Mauritania (near 15–20°N) records a 5–10% increase in annual mean dust deposition at the surface. Although these values are much lower than proxies that record substantial changes in dust flux into the Atlantic during HS1 [*McGee et al*., 2013].

[38] 2. Stronger winds and drier conditions increase North American dust sources, which result in more deposition over Eastern North America, the Bahamas, and along the Gulf Stream in the western North Atlantic. Bahamian speleothems indicate HS were periods of higher iron deposition [*Arienzo et al*., 2011]. Provenance studies have yet to be performed to show whether this indicates and increase in African or North American dust. More observations are needed to determine if other records corroborate these findings.

[39] 3. The southward shift in the ITCZ results in less precipitation and wet dust deposition in the NH tropics and more precipitation and wet dust deposition in the SH tropics. An increase in dust deposition is apparent in the southern tropical Atlantic, southern tropical Pacific, and the Amazon.

[40] 4. Weaker winds lead to less dust emission from glaciogenic sources in Europe. Using a regional climate model, *Sima et al*. [2013] found a weakening of atmospheric circulation over Europe during HS compared to the LGM, and a decrease in dust fluxes throughout most of their domain with an exception in the far eastern domain near 30°E where a 10% increase in dust flux occurs. These changes are consistent with our results.

[41] *McGee et al*. [2013] calculated eolian fluxes at six sediment cores located between 19 and 31°N in the northeastern Atlantic. Core GC68 (at 20°N) shows a 2.5 increase

in dust flux during HS1 compared to the mean 0–2 ka dust flux, which is a minimum estimate as bioturbation may have reduced the peak. Core GC49 (23°N) shows just a muted rise in dust flux, which may be due to either bioturbation or higher dust fluxes may have been limited to regions south of 23°N. Although our model does not simulate coarse grain dust particles, we would also expect the flux of fine particles to increase, since dust emissions scale with wind speed. Our LGM Hose simulation results show a small increase in dust deposition over a narrow region between 10 and 20°N, but this signal appears to be too weak.

[42] *Collins et al*. [2013] recently argued that North African dust sources shifted southward into the Sahel region during the last HS. We found that by perturbing the soil erodibility over the Sahel, dust mobilization, and deposition over the NTA increased. With a modest 10% increase in the area averaged North African soil erodibility, we simulated a 1.25–1.75 increase in dust deposition tropical Atlantic Ocean between 10°S and 15°N.

[43] *Yoshioka et al*. [2007] analyzed the role of dust radiative forcing on African climate and found that it leads to a weaker West African monsoonal flow and a southward displacement of the AEJ, both of which contribute to drying over the Sahel region. Our analysis of the dust-climate feedback shows that dust amplifies the climate response to HS by amplifying the cooling over the North Atlantic and exacerbating the aridity in Africa, the Arabian Sea, and India. This suggests that mismatches between other simulations and proxy data [*Mulitza et al*., 2008; *Kageyama et al*., 2009; *Thomas et al*., 2009] may be due to the lack of dust-climate feedbacks. In the Northern Hemisphere, these changes are consistent with drought throughout the Afro-Asian monsoon region that *Stager et al*. [2011] argued for, and suggest that dust emission, transport, and deposition may be one mechanism in which the signatures of Heinrich stadials are carried out of the Atlantic basin.

[44] Much of these changes do not have observations to verify if they are accurate, but a more detailed comparison of the model to available observations is the subject of future work.

[45] **Acknowledgments.** NSF paleoclimate program. Knight foundation. vS.A. and N.M. would like to acknowledge the support of NSF-0932946 and 1003509. We would like to acknowledge high-performance computing support from Yellowstone (ark:/85065/d7wd3xhc) provided by NCAR's Computational and Information Systems Laboratory, sponsored by the National Science Foundation. The authors would also like to thank three anonymous reviewers for their constructive and insightful comments.

References

Alley, R. B. (2007), Wally was right: Predictive ability of the north Atlantic "conveyor belt" hypothesis for abrupt climate change, *Annu. Rev. Earth Planet. Sci.*, *35*, 241–272, doi:10.1146/annurev.earth.35.081006.131524.

Arienzo, M., P. K. Swart, H. Vonhof, K. Broad, A. C. Clement, A. Eisenhauer, and B. Kakuk (2011), Temporal variability of precipitation and temperature across Heinrich events from a Bahamian stalagmite, AGU, Annual Meeting, San Francisco, Calif.

Bard, E., F. Rostek, J.-L. Turon, and S. Gendreau (2000), Hydrological impact of Heinrich events in the subtropical northeast Atlantic, *Science*, *289*, 1321–1324.

Barker, S., P. Diz, M. J. Vautravers, J. Pike, G. Knorr, I. R. Hall, and W. S. Broecker (2009), Interhemispheric Atlantic seesaw response during the last deglaciation, *Nature*, *457*, 1097–1101.

Bitz, C. M., K. M. Shell, P. R. Gent, D. A. Bailey, G. Danabasoglu, K. C. Armour, M. M. Holland, and J. T. Kiehl (2012), Climate sensitivity of the Community Climate System Model Version 4, *J. Clim.*, doi:10.1175/JCLI-D-11-00290.1.

Bond, G., et al. (1992), Evidence for massive discharges of icebergs into the North Atlantic ocean during the last glacial period, *Nature*, *360*, 245–249, doi:10.1038/360245a0.

Bond, G., W. Broecker, S. Johnsen, J. McManus, L. Labeyrie, J. Jouzel, and G. Bonani (1993), Correlations between climate records from North Atlantic sediments and Greenland ice, *Nature*, *365*, 143–147, doi:10.1038/365143a0.

Bory, A. J. M., and P. P. Newton (2000), Transport of airborne lithogenic material down through the water column in two contrasting regions of the eastern subtropical North Atlantic Ocean, *Global Biogeochem. Cycles*, *14*, 297–315.

Braconnot, P., et al. (2007), Results of PMIP2 coupled simulations of the mid-Holocene and Last Glacial Maximum—Part 1: Experiments and large-scale features, *Clim. Past*, *3*, 261–277, doi:10.5194/cp-3-261-2007.

Brady, E. C., B. L. Otto-Bliesner, J. E. Kay, and N. Rosenbloom (2013), Sensitivity to glacial forcing in the CCSM4, *J. Clim.*, *26*, 1901–1925, doi:10.1175/JCLI-D-11-00416.1.

Briegleb, B. P., and B. Light (2007), A Delta-Eddington multiple scattering parameterization for solar radiation in the sea ice component of the Community Climate System Model, NCAR Tech. Note 472+STR, 100 pp.

Broccoli, A. J., K. A. Dahl, and R. J. Stouffer (2006), Response of the ITCZ to Northern Hemisphere cooling, *Geophys. Res. Lett.*, *33*, L01702, doi:10.1029/2005GL024546.

Broecker, W. S. (1998), Paleocean circulation during the last deglaciation: A bipolar seesaw?, *Paleoceanography*, *13*(2), 119–121, doi:10.1029/97PA03707.

Cakmur, R. V., R. L. Miller, J. Perlwitz, I. V. Geogdzhayev, P. Ginoux, D. Koch, K. E. Kohfeld, I. Tegen, and C. S. Zender (2006), Constraining the magnitude of the global dust cycle by minimizing the difference between a model and observations, *J. Geophys. Res.*, *111*, D06207, doi:10.1029/2005JD005791.

Chapman, M. R., and M. A. Maslin (1999), Low-latitude forcing of meridional temperature and salinity gradients in the subpolar North Atlantic and the growth of glacial ice sheets, *Geology*, *27*, 875–878.

Chen, G., J. Lu, and D. Frierson (2008), The shift in surface westerlies during climate change, *J. Clim.*, *21*, 5942–5959.

Chiang, J. C. H. (2009), The tropics in paleoclimate, in *Annual Review of Earth and Planetary Sciences*, vol. 37, edited by R. Jeanloz and K. H. Freeman, pp. 263–297, Annual Reviews, Palo Alto, Calif.

Chiang, J. C. H., and C. M. Bitz (2005), Influence of high latitude ice cover on the marine Intertropical Convergence Zone, *Clim. Dyn.*, *25*, 477–496, doi:10.1007/s00382-005-0040-5.

Chiang, J. C. H., M. Biasutti, and D. S. Battisti (2003), Sensitivity of the Atlantic Intertropical Convergence Zone to Last Glacial Maximum boundary conditions, *Paleoceanography*, *18*(4), 1094, doi:10.1029/2003PA000916.

Clement A. C., and L. C. Peterson (2008), Mechanisms of abrupt climate change of the last glacial period, *Rev. Geophys.*, *46*, RG4002, doi:10.1029/2006RG000204.

Collins, J. A., A. Govin, S. Mulitza, D. Heslop, M. Zabel, J. Hartmann, U. Röhl, and G. Wefer (2013), Abrupt shifts of the Sahara-Sahel boundary during Heinrich stadials, *Clim. Past*, *9*, 1181–1191, doi:10.5194/cp-9-1181-2013.

Cortijo, E., L. Labeyrie, L. Vidal, M. Vautravers, M. Chapman, J. C. Duplessy, M. Elliot, M. Arnold, J. L. Turon, and G. Auffret (1997), Changes in the sea surface hydrology associated with Heinrich event 4 in the North Atlantic Ocean between 40° and 60°N, *Earth Planet. Sci. Lett.*, *146*, 27–45.

Cuffey, K., and G. D. Clow (1997), Temperature, accumulation, and ice sheet elevation in central Greenland through the last deglacial transition, *J. Geophys. Res.*, *102*, 26,383–26,396.

de Menocal, P., J. Ortiz, T. Guilderson, J. Adkins, M. Sarnthein, L. Baker, and M. Yarusinsky (2000), Abrupt onset and termination of the African humid period: rapid climate responses to gradual insolation forcing, *Quart. Sci. Rev.*, *19*, 347–61.

Dong, B. W., and R. T. Sutton (2002), Adjustment of the coupled ocean–Atmosphere system to a sudden change in the Thermohaline Circulation. *Geophys. Res. Lett.*, *29*(15), 1728, doi:10.1029/2002GL015229.

Evan, A. T., D. J. Vimont, A. K. Heidinger, J. P. Kossin, and R. Bennartz (2009), The role of aerosols in the evolution of tropical north Atlantic Ocean temperature anomalies, *Science*, *324*(5928), 778–781.

Evan, A. T., G. R. Foltz, D. Zhang, and D. J. Vimont (2011), Influence of African dust on ocean atmosphere variability in the tropical Atlantic, *Nat. Geosci.*, *21*, doi:10.1038/ngeo1276.

Evan, A. T., G. R. Foltz, and D. Zhang (2012), Physical response of the tropical–subtropical North Atlantic Ocean to decadal–multidecadal forcing by African dust, *J. Clim.*, *25*, 5817–5829.

Foltz, G. R., and M. J. McPhaden (2008a), Impact of Saharan dust on tropical North Atlantic SST, *J. Clim.*, *21*, 5048–5060.

Foltz, G. R., and M. J. McPhaden (2008b), Trends in Saharan dust and tropical Atlantic climate during 1980–2006, *Geophys. Res. Lett.*, *35*, L20706, doi:10.1029/2008GL035042.

Frierson, D. M. W., and Y.-T. Hwang (2012), Extratropical influence on ITCZ shifts in slab ocean simulations of global warming, *J. Clim.*, *25*, 720–733.

Ganopolski, A., and S. Rahmstorf (2001), Rapid changes of glacial climate simulated in a coupled climate model, *Nature*, *409*, 153–158.

Ganopolski, A., C. Kubatzki, M. Claussen, V. Brovkin, and V. Petoukhov (1998), The influence of vegetation-atmosphere–ocean interaction on climate during the Mid-Holocene, *Science*, *280*(5371), 1916–1919, doi:10.1126/science.280.5371.1916.

Gent, P. R., et al. (2011), The Community Climate System Model version 4, *J. Clim.*, *24*, doi:10.1175/2011JCLI4083.1.

Ginoux, P., M. Chin, I. Tegen, J. M. Prospero, B. N. Holben, O. Dubovik, and S.-J. Lin (2001), Sources and distribution of dust aerosols with the GOCART model, *J. Geophys. Res.*, *106*, 20,255–20,273.

Grousset, F. E., C. Pujol, L. Labeyrie, G. Auffret, and A. Boelaert (2000), Were the North Atlantic Heinrich events triggered by the behaviour of the European ice sheets?, *Geology*, *28*(2), 123–126, doi:10.1130/0091-7613.

Guo, Z., S. Peng, Q. Hao, P. E. Biscaye, Z. An, and T. Liu (2004), Late Miocene–Pliocene development of Asian aridification as recorded in the Red-Earth Formation in northern China, *Global Planet. Change*, *41*(3–4), 135–145.

Heinrich, H. (1988), Origin and consequences of cyclic ice rafting in the Northeast Atlantic Ocean during the past 130,000 years, *Quat. Res.*, *29*(2), 142–152, doi:10.1016/0033-5894(88)90057-9.

Hemming, S. (2004), Heinrich events: Massive late Pleistocene detritus layers of the North Atlantic and their global climate imprint, *Rev. Geophys.*, *42*, RG1005, doi:10.1029/2003RG000128.

Hessler, I., et al. (2010), Millennial scale changes in vegetation records from tropical Africa and South America during the last glacial, *Quat. Sci. Rev.*, *29*, 2882–2899, doi:10.1016/j.quascirev.2009.11.029.

Holland, M. M., D. A. Bailey, B. P. Briegleb, B. Light, and E. Hunke (2012), Improved sea ice shortwave radiation physics in CCSM4: The impact of melt ponds and aerosols on Arctic sea ice*, *J. Clim.*, *25*, 1413–1430.

Huneeus, N., et al. (2011), Global dust model intercomparison in AeroCom phase I, *Atmos. Chem. Phys.*, *11*, 7781–7816.

Hunke, E. C. and W. H. Lipscomb (2008), CICE: The Los Alamos sea ice model user's manual, version 4. Los Alamos National Laboratory, Tech. Report LA-CC-06-012.

Johnson, H. L., and D. P. Marshall (2002), A theory for the surface Atlantic response to thermohaline variability, *J. Phys. Oceanogr.*, *32*, 1121–1132, doi:10.1175/15200485(2002)032<1121:ATFTSA>2.0.CO;2.s.

Jones, C., M. Natalie, and L. Chao (2003), The role of easterly waves on African desert dust transport, *J. Clim.*, *16*, 3617–3628, doi:10.1175/1520-0442(2003)016<3617:TROEWO>2.0.CO;2.

Jullien, E., et al. (2007), Low-latitude "dusty events" vs. high-latitude "icy Heinrich events", *Quat. Res.*, *68*, 379–386, doi:10.1016/j.yqres.2007.07.007.

Just, J., D. Heslop, T. von Dobeneck, T. Bickert, M. J. Dekkers, T. Frederichs, I. Meyer, and M. Zabel (2012), Multiproxy characterization and budgeting of terrigenous end-members at the NW African continental margin, *Geochem. Geophys. Geosyst.*, *13*, Q0AO01, doi:10.1029/2012GC004148.

Kageyama, M., P. J. Valdes, G. Ramstein, C. Hewitt, and U. Wyputta (1999), Northern Hemisphere storm tracks in present day and Last Glacial Maximum climate simulations: A comparison of the European PMIP models, *J. Clim.*, *12*, 742–760.

Kageyama, M., J. Mignot, D. Swingedouw, C. Marzin, R. Alkama, and O. Marti (2009), Glacial climate sensitivity to different states of the Atlantic Meridional Overturning Circulation: Results from the IPSL model, *Clim. Past*, *5*, 551–570.

Kang, S., and J. Lu (2012), Expansion of the Hadley cell under global warming: Winter versus summer, *J. Clim.*, *25*, 8387–8393.

Kang, S. M., D. M. W. Frierson, and I. M. Held (2009), The tropical response to extratropical thermal forcing in an idealized GCM: The importance of radiative feedbacks and convective parameterization, *J. Atmos. Sci.*, *66*(9), 2812–2827, doi:10.1175/2009JAS2924.1.

Kim, J.-H, R. R. Schneider, P. J. Muller, and G. Wefer (2002), Interhemispheric comparison of deglacial sea-surface temperature patterns in Atlantic eastern boundary currents, *Earth Planet. Sci. Lett.*, *194*, 383–393.

Kindler, P., M. Guillevic, M. Baumgartner, J. Schwander, A. Landais, and M. Leuenberger (2013), NGRIP temperature reconstruction from 10 to 120 kyr b2k, *Clim. Past Discuss.*, *9*, 4099–4143, doi:10.5194/cpd-9-4099-2013.

Kok, J. F. (2011), A scaling theory for the size distribution of emitted dust aerosols suggests climate models underestimate the size of the global dust cycle, *Proc. Natl. Acad. Sci.*, *108*(3), 1016–1021.

Kutzbach, J. E., and P. J. Guetter (1986), The influence of changing orbital parameters and surface boundary conditions on climate simulations for the past 18,000 years, *J. Atmos. Sci.*, *43*, 1726–1759.

Lamy, F., J. Kaiser, U. Ninnemann, D. Hebbeln, H. W. Arz, and J. Stoner (2004), Antarctic timing of surface water changes off Chile and Patagonian ice sheet response, *Science*, *304*, 1959–1962, doi:10.1126/science.1097863.

Lamy, F., J. Kaiser, H. W. Arz, D. Hebbeln, U. S. Ninnemann, O. Timm, A. Timmermann, and J. R. Toggweiler (2007), Modulation of the bipolar seesaw in the Southeast Pacific during Termination 1, *Earth Planet. Sci. Lett.*, *259*, 400–413.

Lawrence, P. J., and T. N. Chase (2007), Representing a new MODIS consistent land surface in the Community Land Model (CLM 3.0), *J. Geophys. Res.*, *112*, G01023, doi:10.1029/2006JG000168.

Lawrence, C. R., and J. C. Neff (2009), The contemporary physical and chemical flux of Aeolian dust: A synthesis of direct measurements of dust deposition, *Chem. Geol.*, *257*, 46–63.

Lawrence, P. J., et al. (2012), Simulating the biogeochemical and biogeophysical impacts of transient land cover change and wood harvest in the community climate system model (CCSM4) from 1850 to 2100, *J. Clim.*, *25*, 3071–3095.

Lee, S., and H.-K. Kim (2003), The dynamical relationship between subtropical and eddy-driven jets, *J. Atmos. Sci.*, *60*, 1490–1503.

Lee, S.-Y., J. C. H. Chiang, K. Matsumoto, and K. S. Tokos (2011), Southern Ocean wind response to North Atlantic cooling and the rise in atmospheric CO_2: Modeling perspective and paleoceanographic implications, *Paleoceanography*, *26*, PA1214, doi:10.1029/2010PA002004.

Lorenz, D. J., and E. T. DeWeaver (2007), The tropopause height and the zonal wind response to global warming in the IPCC scenario integrations, *J. Geophys. Res.*, *112*, D10119, doi:10.1029/2006JD008087.

Lu, J., G. Chen, and D. Frierson (2008), Response of the zonal mean atmospheric circulation to El Nino versus global warming, *J. Clim.*, *21*, 5835–5851.

Maher, B. A., and K. E. Kohfeld (2009), DIRTMAP version 3. LGM and late Holocene aeolian fluxes from Ice cores, Marine Sediment Traps, Marine Sediments, and Loess Deposits, http://www.lec.lancs.ac.uk/dirtmap3.

Mahowald, N. M., D. R. Muhs, S. Levis, P. J. Rasch, M. Yoshioka, C. S. Zender, and C. Luo (2006), Change in atmospheric mineral aerosols in response to climate: Last glacial period, preindustrial, and doubled carbon dioxide climates, *J. Geophys. Res.*, *111*, D10202, doi:10.1029/2005JD006653.

Mahowald, N. M., et al. (2010), Observed 20th century desert dust variability: Impact on climate and biogeochemistry, *Atmos. Chem. Phys.*, *10*, 10,875–10,893, doi:10.5194/acp-10-10875-2010.

Mahowald, N., S. Albani, S. Engelstaedter, G. Winckler, and M. Goman (2011), Model insight into glacial–interglacial paleodust records, *Quat. Sci. Rev.*, *30*(7–8), 832–854, doi:10.1016/j.quascirev.2010.09.007.

Manabe, S., and R. J. Stouffer (1993), Century-scale effects of increased atmospheric CO2 on the ocean– Atmosphere system, *Nature*, *364*, 215–218.

Martinez Avellaneda, N., N. Serra, P. J. Minnett, and D. Stammer (2010), Response of the eastern subtropical Atlantic SST to Saharan dust: A modeling and observational study, *J. Geophys. Res.*, *115*, C08015, doi:10.1029/2009JC005692.

Martínez-Garcia, A., A. Rosell-Melé, S. L. Jaccard, W. Geibert, D. M. Sigman, and G. H. Haug (2011), Southern Ocean dust-climate coupling during the past four million years, *Nature*, *476*, 312–315, doi:10.1038/nature10310.

Masson-Delmotte, V., J. Jouzel, A. Landais, M. Stievenard, S. J. Johnsen, J. W. C. White, M. Werner, A. Sveinbjornsdottir, and K. Fuhrer (2005), GRIP deuterium excess reveals rapid and orbital-scale changes in Greenland moisture origin, *Science*, *309*(5731), 118–121.

McGee, D., P. B. deMenocal, G. Winckler, J. B. W. Stuut, and L. I. Bradtmiller (2013), The magnitude, timing, and abruptness of changes in North African dust deposition over the last 20,000 yr, *Earth Planet. Sci. Lett.*, *371–372*, 163–176.

McManus, J. F., R. Francois, J. M. Gherardi, L. D. Keigwin, and S. Brown-Leger (2004), Collapse and rapid resumption of Atlantic meridional circulation linked to deglacial climate changes, *Nature*, *428*, 834–837, doi:10.1038/nature02494.

Michel, P. (1973), Les bassins des fleuves Se´ne´galet Gambie, in E ´ tude Ge´omorphologique, rep., Inst. de Rech. pour le De´v., Paris.

Miller, R., I. Tegen, and J. Perlwitz (2004), Surface radiative forcing by soil dust aerosols and the hydrologic cycle, *J. Geophys. Res.*, 109, D04203, doi:10.1029/2003JD004085.

Mulitza, S., M. Prange, J.-B. Stuut, M. Zabel, T. von Dobeneck, A. C. Itambi, J. Nizou, M. Schulz, and G. Wefer (2008), Sahel megadroughts triggered by glacial slowdowns of Atlantic meridional overturning, *Paleoceanography*, *23*, PA4206, doi:10.1029/2008PA001637.

Neale, R. B., J. Richter, S. Park, P. H. Lauritzen, S. J. Vavrus, P. J. Rasch, and M. Zhang (2013), The mean climate of the Community Atmosphere Model (CAM4) in forced SST and fully coupled experiments, *J. Clim.*, *26*, 5150–5168.

Niedermeyer, E. M., M. Prange, S. Mulitza, G. Mollenhauer, E. Schefub, and M. Schulz (2009) Extratropical forcing of Sahel aridity during

Heinrich stadials, *Geophys. Res. Lett.*, *36*, L20707, doi:10.1029/2009GL039687.
Otto-Bliesner, B. L., and E. C. Brady (2010), The sensitivity of the climate response to the magnitude and location of freshwater forcing: Last glacial maximum experiments, *Quat. Sci. Rev.*, *29*, 56–73.
Otto-Bliesner, B. L., E. C. Brady, G. Clauzet, R. Tomas, S. Levis, and Z. Kothavala (2006), Last Glacial Maximum and Holocene Climate in CCSM3, *J. Clim.*, *19*, 2526–2544.
Peterson, L. C., G. H. Haug, K. A. Hughen, and U. Röhl (2000), Rapid changes in the hydrologic cycle of the tropical Atlantic during the last glacial, *Science*, *290*, 1947–1951, doi:10.1126/science.290.5498.1947.
Prospero, J. M., P. Ginoux, O. Torres, S. E. Nicholson, and T. E. Gill (2002), Environmental characterization of global sources of atmospheric soil dust identified with the NIMBUS 7 Total Ozone Mapping Spectrometer (TOMS) absorbing aerosol product, *Rev. Geophys.*, *40*(1), 1002, doi:10.1029/2000RG000095.
Rahmstorf, S. (2002), Ocean circulation and climate during the past 120,000 years, *Nature*, *419*, 207–214.
Rashid, H., B. P. Flower, R. Z. Poore, and T. M. Quinn (2007), A ~25 ka Indian Ocean monsoon variability record from the Andaman Sea, *Quat. Sci. Rev.*, *26*, 2586–2597.
Rashid, H., E. England, L. Thompson, and L. Polyak (2011), Late glacial to Holocene Indian summer monsoon variability based upon sediment records taken from the Bay of Bengal, *Terr. Atmos. Ocean. Sci.*, *22*, 215–228.
Reid, J. S., et al. (2003), Comparison of size and morphological measurements of coarse mode dust particles from Africa, *J. Geophys. Res.*, *108*, D19, 8593, doi:10.1029/2002JD002485.
Rühlemann, C., S. Mulitza, P. J. Mueller, G. Wefer, and R. Zahn (1999), Warming of the tropical Atlantic Ocean and slowdown of thermohaline circulation during the last deglaciation, *Nature*, *402*, 511–514.
Schulz, H., U. von Rad, and H. Erlenkeuser (1998), Correlations between Arabian Sea and Greenland climate oscillations of the past 110,000 years, *Nature*, *393*, 54–57.
Schuster, M., P.Duringer, J.-F. Ghienne, P. Vignaud, H. T. Mackaye, A. Likius, and M. Brunet (2006), The Age of the Sahara Desert, *Science*, *311*(5762), 821, doi:10.1126/science.1120161.
Shao, Y., K.-H. Wyrwoll, A. Chappell, J. Huang, Z. Lin, G. H. McTainsh, M. Mikami, T. Y. Tanaka, X. Wang, and S. Yoon (2011), Dust cycle: An emerging core theme in Earth system science, *Aeol. Res.*, *2*, 181–204.
Sima, A., M. Kageyama, D.-D. Rousseau, G. Ramstein, Y. Balkanski, P. Antoine, and C. Hatte (2013), Modeling dust emission response to North Atlantic millennial-scale climate variations from the perspective of East European MIS 3 loess deposits, *Clim. Past.*, *9*, 1385–1402, doi:10.5194/cp-9-1385-2013.
Sirocko, F., D. Garbe-Schönberg, and C. Devey (2000), Processes controlling trace element geochemistry of Arabian Sea sediments during the last 25,000 years, *Global Planet. Change*, *26*(1–3), 217–303, doi:10.1016/S0921-8181(00)00046-1.
Speich, S., B. Blanke, and W. Cai (2007), Atlantic meridional overturning circulation and the Southern Hemisphere supergyre, *Geophys. Res. Lett.*, *34*, L23614, doi:10.1029/2007GL031583.
Stager, J. C., D. B. Ryves, B. M. Chase, and F. S. R. Pausata (2011), Catastrophic drought in the Afro-Asian Monsoon Region During Heinrich Event 1, *Science*, *331*, 1299, doi:10.1126/science.1198322.
Stocker, T. F. (1998), The seesaw effect, *Science*, *282*, 61–62.
Stocker, T. F., and S. J. Johnsen (2003), A minimum thermodynamic model for the biopolar seesaw, *Paleoceanography*, *18*(4), 1087, doi:10.1029/2003PA000920.
Stouffer, R. J., et al. (2006), Investigating the causes of the response of the thermohaline circulation to past and future climate changes, *J. Clim.*, *19*, 1365–1387.
Tegen, I. (2003), Modeling soil dust aerosol in the climate system: An overview, *Quat. Sci. Rev.*, *22*, 1821–1834.
Thomas, D. S. G., R. Bailey, P. A. Shaw, J. A. Durcan, and J. S. Singarayer (2009), Late quaternary highstands at Lake Chilwa, Malawi: Frequency, timing and possible forcing mechanisms in the last 44 ka, *Quat. Sci. Rev.*, *28*, 526–539.
Tjallingii, R., M. Claussen, J.-B. W. Stuut, J. Fohlmeister, A. Jahn, T. Bickert, F. Lamy, and U. Rohl (2008), Coherent high- and low-latitude control of the northwest African hydrological balance, *Nat. Geosci.*, *1*, 670–675, doi:10.1038/ngeo289.
Turney, C. S. M., et al. (2006), Climate variability in the southwest Pacific during the Last Termination (20–10 kyr BP), *Quat. Sci. Rev.*, *25*, 886–903.
Van der Kaars, S., D. Penny, J. C. Tibby, J. Fluin, R. A. C. Dam, and P. Suparan (2001), Late Quarternary palaeoecology, palynology and palaeolimnology of a tropical lowland swamp: Rawa Danau, West-Java, Indonesia, *Palaeogeogr. Palaeoclimatol. Palaeoecol.*, *171*, 185–212, doi:10.1016/S0031-0182(01)00245-0.
Vellinga, M., and R. A. Wood (2002), Global climate impacts of a collapse of the Atlantic thermohaline circulation, *Clim. Change*, *54*, 251–267.
Vidal, L., L. Labeyrie, E. Cortijo, M. Arnold, J. Duplessy, E. Michel, S. Becque, and T. van Weering (1997), Evidence for changes in the North Atlantic DeepWater linked to meltwater surges during the in the North Atlantic DeepWater linked to meltwater surges during the Heinrich events, *Earth Planet. Sci. Lett.*, *146*, 13–27.
Wang, X., A. S. Auler, R. L. Edwards, H. Cheng, P. S. Cristalli, P. L. Smart, D. A. Richards, and C.-C. Shen (2004), Wet periods in northeastern Brazil over the past 210 kyr linked to distant climate anomalies, *Nature*, *432*, 740–743.
Wang, C., S. Dong, A. T. Evan, G. R. Foltz, and S.-K. Lee (2012), Multidecadal Co-variability of North Atlantic Sea Surface Temperature, African Dust Sahel Rainfall and Atlantic Hurricanes, *J. Clim.*, *25*, 5405–5415.
Yin, J. H. (2005), A consistent poleward shift of the storm tracks in simulations of 21st century climate, *Geophys. Res. Lett.*, *32*, L18701, doi:10.1029/2005GLO23684.
Yoshioka, M., N. M. Mahowald, A. J. Conley, W. D. Collins, D. W. Fillmore, C. S. Zender, and D. B. Coleman (2007), Impact of desert dust radiative forcing on Sahel precipitation: Relative importance of dust compared to sea surface temperature variations, vegetation changes, and greenhouse gas warming, *J. Clim.*, *20*, 1445–1467.
Zender, C., H. Bian, and D. Newman (2003a), Mineral dust entrainment and deposition (DEAD) model: Description and 1990s dust climatology, *J. Geophys. Res.*, *108*(D14), 4416, doi:10.1029/2002JD002775.
Zender, C., D. Newman, and O. Torres (2003b), Spatial heterogeneity in aerolian erodibility: Uniform, topographic, geomorphic, and hydrologic hypotheses, *J. Geophys. Res.*, *108*(D17), 4543, doi:10.1029/2002JD003039.
Zhang, R., and T. L. Delworth (2005), Simulated tropical response to a substantial weakening of the Atlantic thermohaline circulation, *J. Clim.*, *18*, 1853–1860, doi:10.1175/JCLI3460.1.
Zhao, M., N. A. S. Beveridge, N. J. Shackleton, M. Sarnthein, and G. Eglinton (1995), Molecular stratigraphy of cores off nortvhwest Africa: Sea surface temperature history over the last 80 ka, *Paleoceanography*, *10*, 661–675.